Pile Bearing Capacity Factors and Soil Crushabiity

Keiji Kuwajima[1]; Masayuki Hyodo[2]; and Adrian F. L. Hyde[3]

Abstract: The existence of large magnitude stresses at the tip of a bearing pile is a well known phenomenon leading to crushing of soil grains and thus affecting pile behavior. Classical foundation design calculations which assume that the soil fails in shear and neglect volume change can be safely used where stress levels or particle strengths prevent crushing, however in the case of weak grains or high foundation stresses consideration should be given to the effects of grain crushing and the resulting volumetric compression. Model pile tests have been carried out in two skeletal carbonate sands and a standard silica sand with the aim of examining the variation of skin friction and end bearing capacities with degree of penetration. The mobilization of the strength of crushable soils requires a much higher strain level while at the same time the end bearing pressure on the model piles exceeded 10 MPa inducing considerable particle breakage. The peak skin friction for all sands occurred at a settlement normalized by pile diameter, S/D, of less than 0.1. At this point the carbonate sands generally had lower skin friction values than the silica sand. Further displacement caused a rapid decrease in skin friction for all three materials. At higher lateral stresses the less crushable Toyoura silica sand generated higher skin frictions. Samples of Chiibishi sand were sectioned and photographed. It was observed that a spherical plastic zone was formed at the base of the pile which expanded with increasing S/D and a degraded layer of broken particles developed around the pile as S/D increased. Large values of the Marsal particle breakage factor were restricted to a zone extending outwards to one pile radius. An end bearing capacity modification factor has been proposed to adapt the conventional bearing capacity equation for soil crushability. This modification factor is a function of soil compressibility and degree of penetration. The factor was shown to decrease with increasing soil compressibility and increase with normalized penetration S/D.

DOI: 10.1061/(ASCE)GT.1943-5606.0000057

CE Database subject headings: Piles; Load bearing capacity; Friction; Sand; Silica; Calcareous soils; Soil compression; Model tests.

Introduction

There exists a large class of crushable geomaterials with weak grains such as carbonate sands, volcanic soils, decomposed granites, and mica-rich sands. However particle crushing is not limited to these materials and has been shown to occur over a wide range of stress conditions including monotonic and cyclic, drained, and undrained triaxial shearing (Miura and O-hara 1979; Bopp and Lade 1997; Hyodo et al. 1996; Nakata et al. 1999); direct shear (Tarantino and Hyde 2005; Coop et al. 2004) and one-dimensional compression (Nakata et al. 2001a, b). Coop (1990), testing a crushable sand, demonstrated that the shape of the one-dimensional compression curve is similar for all soils ranging from clays to sands, suggesting that particle crushing is common for all granular materials. It has also been demonstrated using fractal mechanics that yielding under a one-dimensional compressive stress is related to the phenomenon of particle crushing for granular materials (McDowell and Bolton 1998; McDowell and Daniell 2001; McDowell and Harireche 2002). Bolton (1986) linked particle crushing to the reduction in peak strength, a suppression of dilatancy, and an increase in compressibility, while Golightly and Hyde (1988) showed that for highly crushable materials, peak strengths are reached at relatively high strain levels.

Various combinations of stress can exist in a soil adjacent to a pile and a given soil element could be subjected to any of these during pile driving and final loading (White and Bolton 2004). This could include cyclic triaxial shear with rotation of principal stresses, static triaxial shear, and simple shear adjacent to the pile shaft. There have been some studies of the effect of particle crushing on the in situ behavior of foundations. For example, the existence of large magnitude stresses at the tip of a bearing pile is a well-known phenomenon leading to crushing of soil grains and thus affecting pile behavior (Yasufuku and Hyde 1995; Tanaka et al. 1995). White and Bolton (2004) carried out a series of plane strain calibration chamber tests to examine the interface layer adjacent to a driven pile shaft and showed that it comprised soil particles broken as they passed the zone below the pile tip. This interface zone contracted further during pile penetration leading to a degradation of shaft friction.

Classical foundation design methods have evolved from limit equilibrium and plasticity solutions based on rigid plastic failure mechanisms that neglect volume compressibility arising from crushing. These methods can be safely used where stress levels or particle strengths prevent crushing; however in the case of weak grains or high foundation stresses consideration should be given to the effects of grain crushing. The study of the mechanism for bearing capacity in crushable materials is complicated by the rearrangement and densification of the soil structure under crushing.

[1]Researcher, Tokuyama College of Technology, 3538 Takajo, Kume, Shunan City, Yamaguchi Prefecture 745-8585, Japan. E-mail: kuwajima@tokuyama.ac.jp

[2]Professor, Dept. of Civil Engineering, Yamaguchi Univ., Tokiwadai 2-16-1, Ube 755-8611, Japan. E-mail: hyodo@yamaguchi-u.ac.jp

[3]Professor of Geotechnical Engineering, Dept. of Civil and Structural Engineering, Univ. of Sheffield, Mappin St., Sheffield S1 3JD, U.K. (corresponding author). E-mail: a.f.l.hyde@sheffield.ac.uk

Note. This manuscript was submitted on October 22, 2007; approved on November 6, 2008; published online on February 21, 2009. Discussion period open until December 1, 2009; separate discussions must be submitted for individual papers. This paper is part of the ***Journal of Geotechnical and Geoenvironmental Engineering***, Vol. 135, No. 7, July 1, 2009. ©ASCE, ISSN 1090-0241/2009/7-901–913/$25.00.

Table 1. Physical Properties of Sands

Material	Specific gravity G_s	Maximum particle size D_{max} (mm)	50% particle size D_{50} (mm)	Particle size relative to model pile diameter D/D_{50}	Void ratio e_{max}	Void ratio e_{min}	Carbonate content $CaCO_3$ (%)
Chiibishi sand	2.83	2.0	0.68	44	1.574	0.983	96
Dogs Bay sand	2.72	2.0	0.22	136	2.451	1.621	94
Toyoura sand	2.64	1.5	0.25	120	0.973	0.635	—

Yasufuku and Hyde (1995) developed a spherical cavity expansion analysis for the end bearing capacity of piles in crushable soils. Pushing model piles to a maximum penetration of one pile diameter, Tanaka et al. (1995) performed model pile skin friction tests using a pile with a surface roughness of 15 μm. Each of the above authors investigated the bearing capacity of piles using silica and carbonate sands. In this work the writers have used a roughened pile representing a nondisplacement or bored pile which was then penetrated to a maximum of three pile diameters. Measurements have been made of the degree of particle crushing in the vicinity of the pile, and the development of the displacement bulb ahead of the pile, and the mobilized bearing capacity and shaft resistance.

Material Properties

Model pile tests were carried out in three materials: Chiibishi sand, a skeletal carbonate beach sand from Okinawa, Japan; Dogs Bay sand, a skeletal carbonate beach sand from the west coast of Eire, which has been used by many researchers (Golightly and Hyde 1988; Coop 1990; Yasufuku and Hyde 1995; White and Bolton 2004; Tarantino and Hyde 2005); and Toyoura sand, a Japanese standard silica sand widely used for research. The physical properties of the materials are shown in Table 1 and grain size distributions in Fig. 1. The coefficients of uniformity ($U_c = D_{60}/D_{10}$) and range of void ratios are shown in Fig. 2 for each material tested and some additional materials for comparison such as: Quiou sand, Golightly (1989); Shirasu a volcanic soil; Masado, a decomposed granite (Hyodo et al. 1998); and another silica sand, Aio sand (Hyodo et al. 2002). It can be seen that crushable soils such as Quiou, Dogs Bay, and Chiibishi sands have a large range of void ratios compared to silica sands such as Toyoura and Aio. Fig. 3 shows a comparison of grain shape and variability for the three sands used for the model pile tests. It can be seen that Toyoura sand particles are subrounded while the Chiibishi and Dogs bay sand particles vary from platey to biogenic rounded.

Shear Behavior of Crushable Soils

Consolidated drained triaxial tests were carried out on the three sands. Specimens were prepared to 90% relative density and tests were performed at confining stresses between 50 and 400 kPa. Figs. 4(a–c) show deviator stress and volumetric strain against axial strain for the three materials. The peak deviator stress was reached at an axial strain of $\leqslant 5\%$ for the silica Toyoura sand, in contrast to the carbonate sands where peak stresses were reached at axial strains of more than 20% in some cases. Fig. 5 shows the variation of the peak secant friction angle ϕ_{sp} as a function of confining pressure. It can be seen that the friction angle for the Chiibishi sand is consistently higher than either the Dogs Bay or Toyoura. This confirms the observation by previous researchers that higher friction angles are obtained for carbonate sands compared to silica sands (Coop 1990; Hyde 1994). In addition it can be seen that the variation in peak friction angle with confining stress is greater for the Dogs Bay sand than for Chiibishi or Toyoura. Previous work by researchers such as Golightly (1989), Coop (1990), and Airey and Fahey (1991) showed that the curvature of the Mohr–Coulomb envelope for peak stresses is related to particle crushing while Tarantino and Hyde (2005) also demonstrated curvature of the critical state ϕ value due to particle breakage in direct shear tests. From this we can infer that the grains of the Dogs Bay sand are more susceptible to breakage and are thus weaker than those of the Chiibishi sand. At the highest confining stress of 400 kPa the peak deviator stress was reached

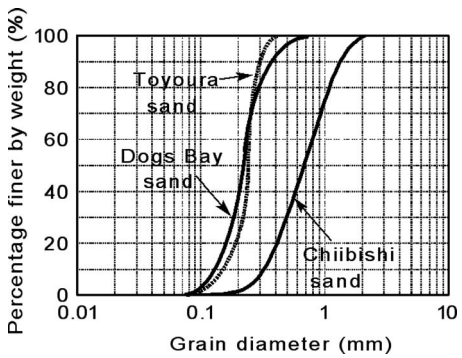

Fig. 1. Grain-size distributions

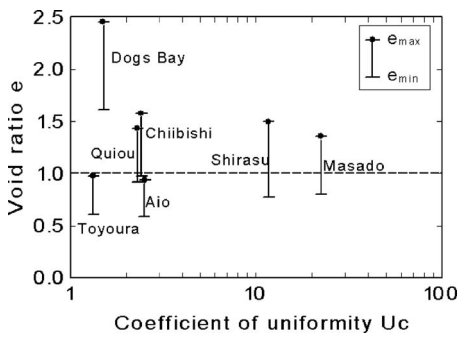

Fig. 2. Range of void ratios

J. Geotech. Geoenviron. Eng., 2009, 135(7): 901-913

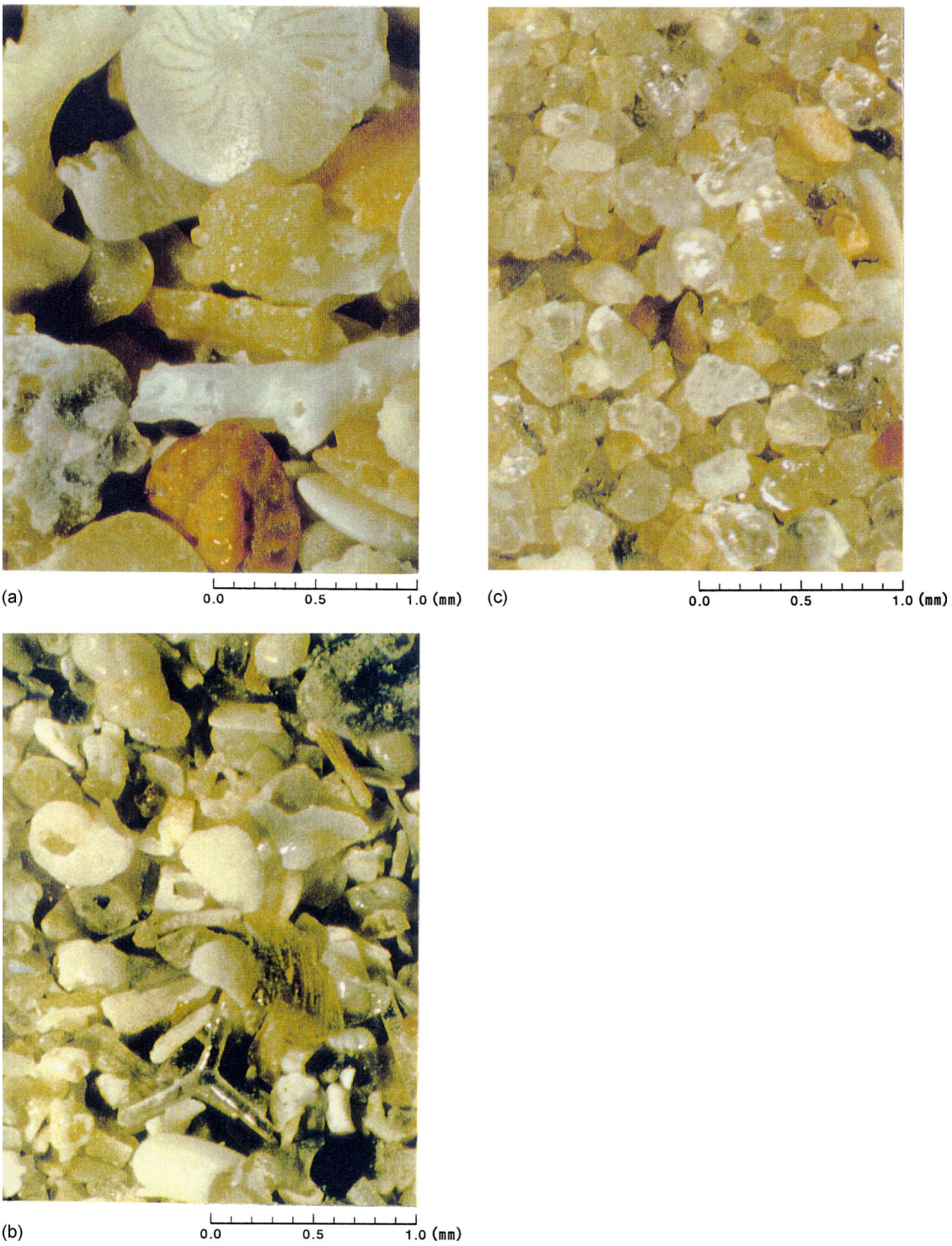

Fig. 3. (a) Chiibishi sand; (b) Dogs Bay sand; and (c) Toyoura sand

at axial strains of 5, 14, and more than 20% for Toyoura, Chiibishi, and Dogs Bay sands, respectively, which together with the overall decreasing tendency to dilate for each sand is a further indicator of the relative grain crushing and strengths. It should be noted that mobilization of the strength of crushable soils requires a much higher strain level which is an important consideration in bearing capacity problems.

Bearing Capacity of Piles in Crushable Soils

Experimental Methodology

Model tests have been performed in order to better understand the bearing capacity of piles. The model pile is shown in Fig. 6 and the testing apparatus and specimen can be seen in Fig. 7. The pile was made from roughened steel with a diameter of 30 mm, length

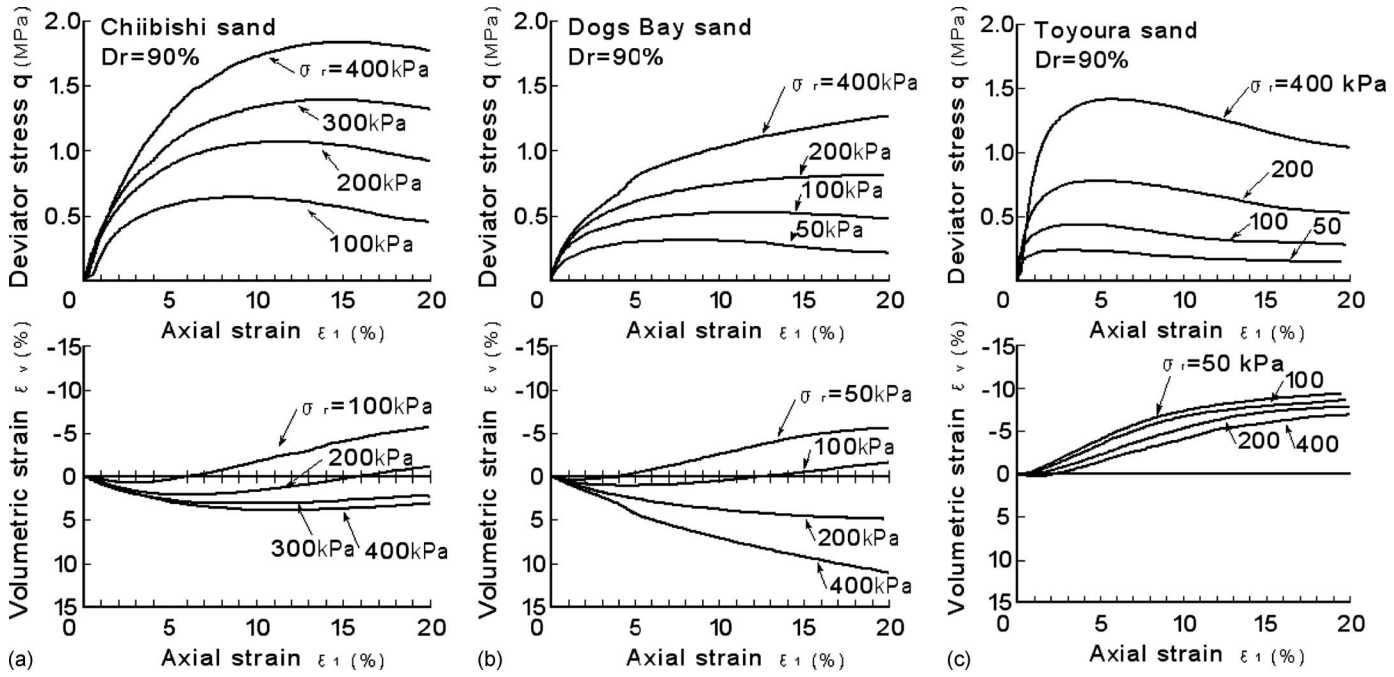

Fig. 4. (a) Stress-strain characteristics for Chiibishi sand; (b) stress-strain characteristics for Dogs Bay sand; and (c) stress-strain characteristics for Toyoura sand

of 240 mm, and surface roughness of 600 μm. Sand specimens were compacted around the model pile. Specimens whose dimensions were 300 mm diameter by 400 mm height were prepared in a mold by tamping 40 × 1 cm layers to a relative density of 90%. The soil was confined in a latex membrane and lateral and vertical pressures were applied independently using air pressure. The model pile diameter of 30 mm corresponded to overall 10% of the soil sample diameter. Consideration was given to the influence of grain size effects on interface friction and end bearing capacity. Values of the ratio of pile diameter to grain size D_{50} were between 44 and 136 (Table 1). These were large enough for the grain size effects to be minimal although the value of 44 for Chiibishi sand could be regarded as marginal (Garnier et al. 2007). Penetration was from the base of the sample and the model pile consisted of two sleeved concentric tubes in order to measure skin friction and

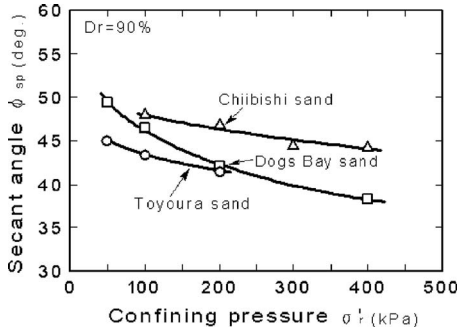

Fig. 5. Variation of peak secant friction angle with confining pressure

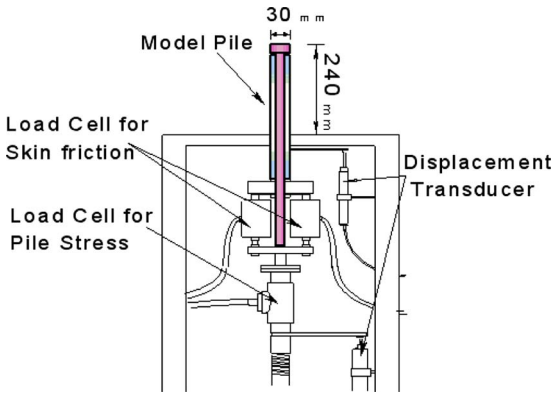

Fig. 6. Model pile with skin friction and total load cells

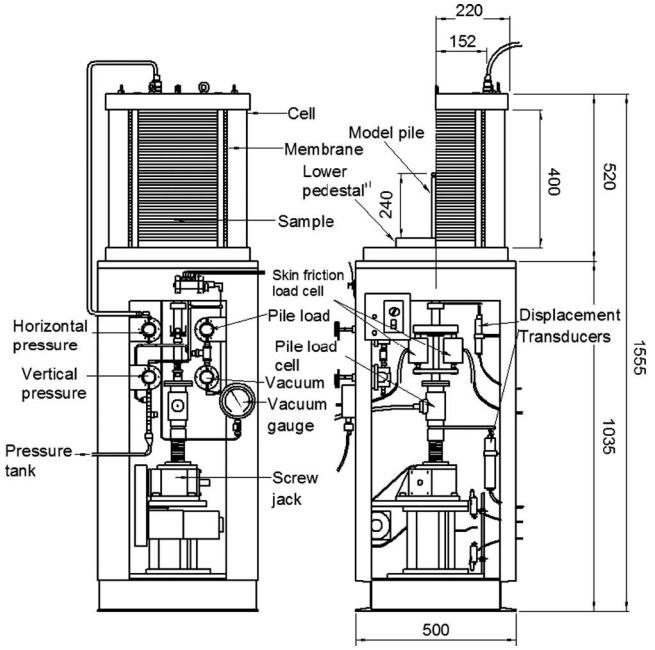

Fig. 7. Testing apparatus and soil specimen

J. Geotech. Geoenviron. Eng., 2009, 135(7): 901-913

Table 2. Pile Testing Program

Principal stress ratio K	0.5	0.5	1.0	1.0
Vertical stress σ_v' (kPa)	200	400	100	300
Horizontal stress σ_h' (kPa)	100	200	100	300
Mean effective principal stress σ_m (kPa)	133	267	100	300

end bearing capacity independently (Fig. 6). Independent readings were taken of skin friction and total load from which the end bearing capacity was determined by subtraction of the skin friction from the total load. The application of independent vertical and lateral stress allowed various stress ratios, $K=\sigma_h/\sigma_v$, to be applied.

The penetration of the model pile was displacement-controlled at 0.1 mm/min. Penetration of the pile from the base allowed for easier sample preparation with less disturbance and better centering of the pile. Sample deposition created a two-dimensional horizontally layered anisotropy. Thus pile penetration from the base was perpendicular to the layering in the same way as top down penetration. Yasufuku et al. (1994) carried out tests showing that base penetration produced identical results to top penetration.

Tests were performed using Toyoura, Chiibishi, and Dogs Bay sand samples prepared to a relative density of 90% and the applied soil stress conditions are given in Table 2. Two stress ratio values, K, of 0.5 and 1.0 were used for vertical stresses of 100–400 kPa.

Pile End Bearing Capacity

End bearing and skin friction values plotted against normalized displacement S/D (where S is displacement or pile settlement and D is pile diameter) are shown in Figs. 8 and 9 respectively. Tests were carried out in three stages, with pile loading being reduced to zero at settlement to pile diameter S/D ratios, of 1.0, 2.0, and 3.0. Fig. 8 shows the maximum curvature representing yield of the end bearing load versus settlement relation is more marked for Toyoura sand and occurs well before a normalized displacement of $S/D=1.0$. In the case of the more crushable carbonate sands the curvature and yielding is less pronounced. Even when the

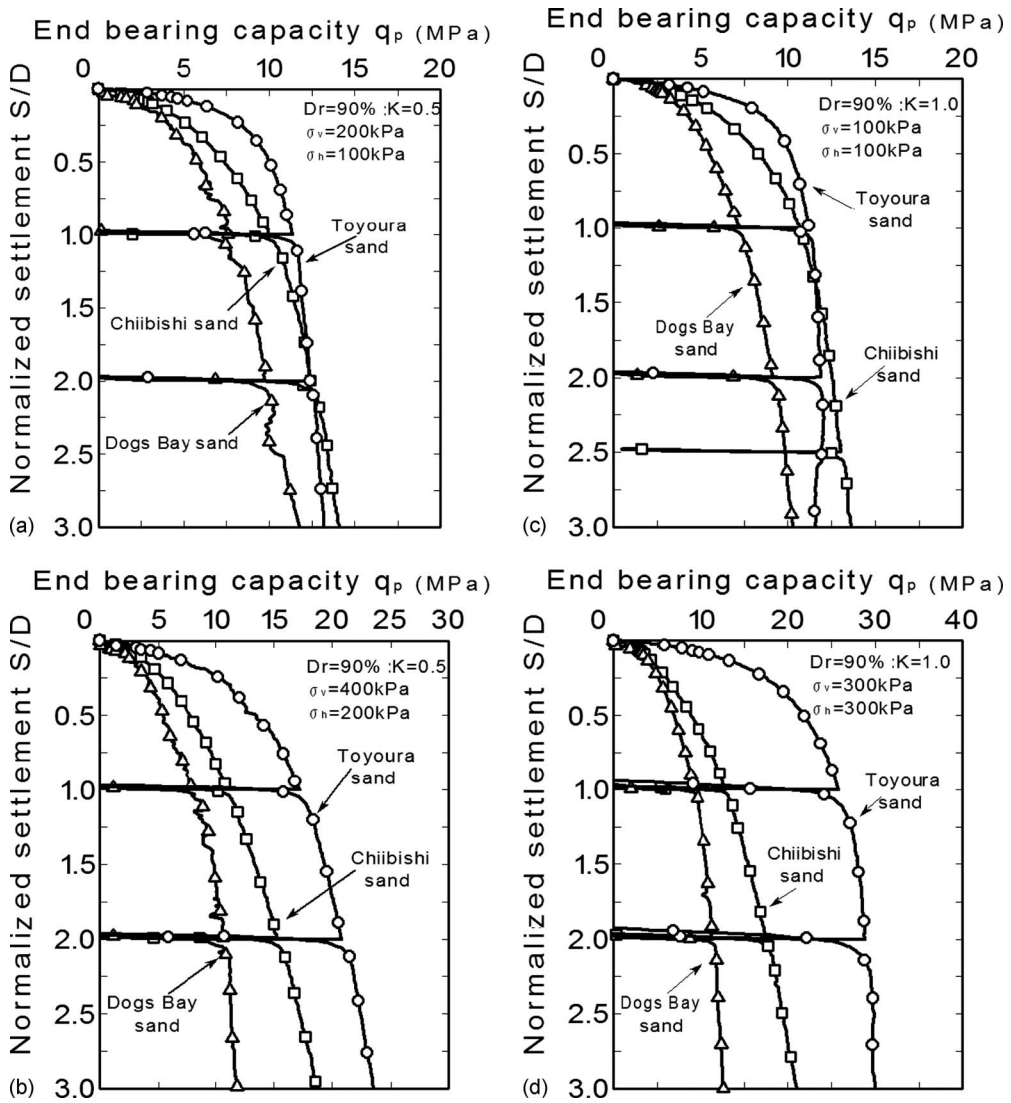

Fig. 8. (a) End bearing capacity versus normalized settlement, $\sigma_v=200$ kPa, $K=0.5$; (b) end bearing capacity versus normalized settlement, $\sigma_v=400$ kPa, $K=0.5$; (c) end bearing capacity versus normalized settlement, $\sigma_v=100$ kPa, $K=1.0$; and (d) end bearing capacity versus normalized settlement, $\sigma_v=300$ kPa, $K=1.0$

J. Geotech. Geoenviron. Eng., 2009, 135(7): 901-913

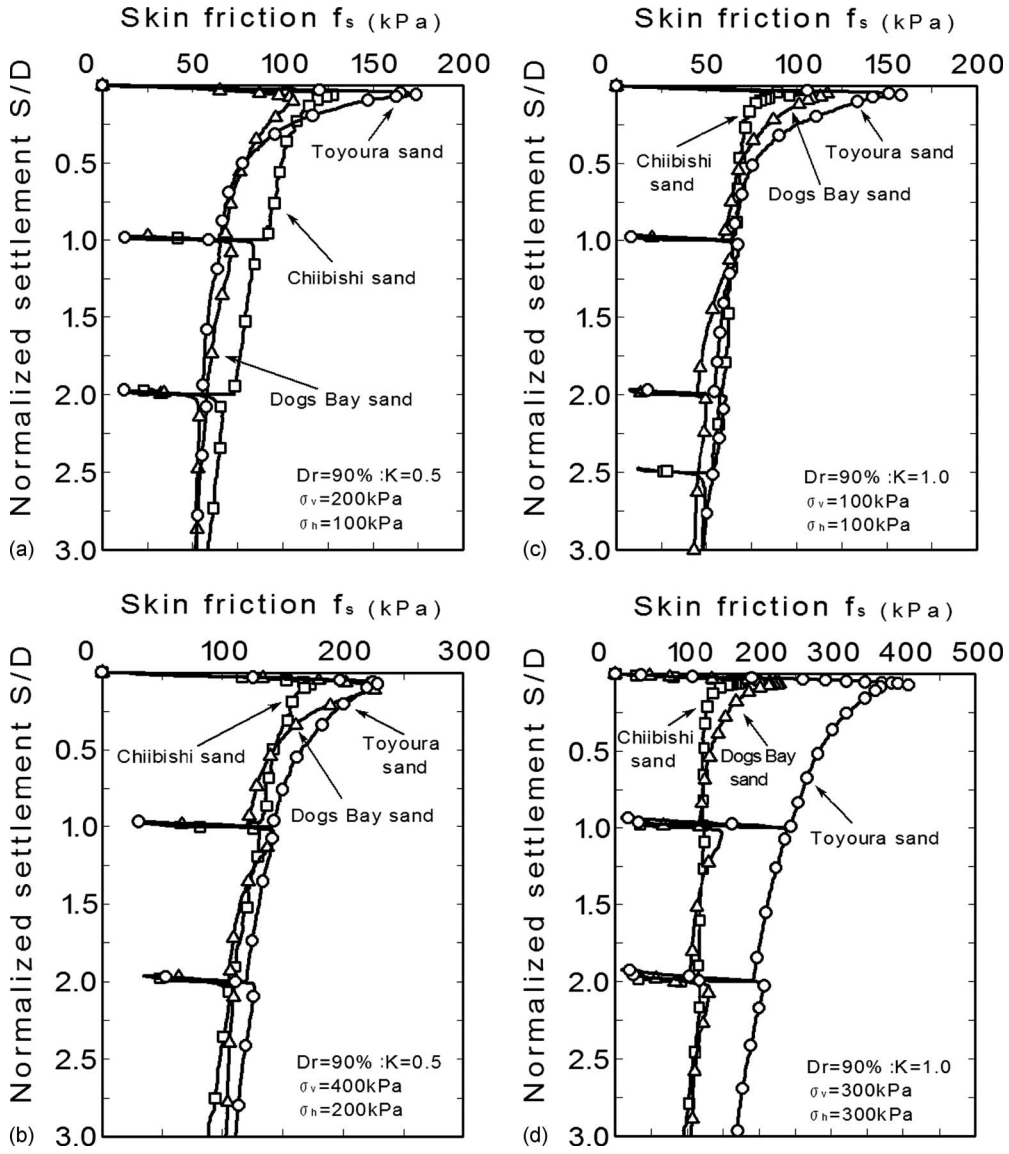

Fig. 9. (a) Skin friction versus normalized settlement, $\sigma_v = 200$ kPa, $K = 0.5$; (b) skin friction versus normalized settlement, $\sigma_v = 400$ kPa, $K = 0.5$; (c) skin friction versus normalized settlement, $\sigma_v = 100$ kPa, $K = 1.0$; and (d) skin friction versus normalized settlement, $\sigma_v = 300$ kPa, $K = 1.0$

tests were taken to a settlement of 300% of the pile diameter there was no clear limiting load for these materials. In the case of Toyoura sand and a K value of 1.0, a limiting end bearing capacity was reached. In Figs. 8(a and c) for low confining pressures, Toyoura sand initially had a higher bearing capacity but for $S/D > 2$ it was exceeded by Chiibishi sand. On the other hand for higher confining pressures shown in Figs. 8(b and d), the bearing capacity of Toyoura sand remained the largest even at large normalized displacements. Under low confining stress as shown in Figs. 8(a and c), the behavior of Chiibishi and Toyoura sands are very similar. However, at high confining stresses the bearing capacity decreases with increasing crushability of the sands and there is a marked distinction in behavior for each of the three materials.

The patterns of end bearing behavior closely match the triaxial tests where peak strength was reached at relatively high strains for Chiibishi sand and no clear peak was achieved for Dogs Bay sand. The end bearing pressure exceeding 10 MPa in all cases combined with the significant shear strains as the soil was forced to flow around the pile tip would have caused considerable particle breakage particularly in the more crushable materials (Coop 1990; Coop et al. 2004). It is important to take this into account when formulating the bearing capacity of a pile.

Pile Skin Friction

Figs. 9(a–d) show the corresponding skin friction plots. Tanaka et al. (1995) in a previous study using the same apparatus used a smooth pile (surface roughness 15 μm). The work described here in contrast demonstrated much higher skin friction and associated brittle behavior at low displacements. The peak skin friction occurred at a displacement of less than $S/D = 0.1$. At this point the carbonate sands generally had lower skin friction values than the silica sand. Further displacement caused a rapid decrease in skin friction for all three materials. This phenomenon was explained as friction fatigue by White and Bolton (2004) who observed a contracting interface zone consisting of broken particles adjacent to a pile. This mechanism caused further degradation of skin friction

J. Geotech. Geoenviron. Eng., 2009, 135(7): 901-913

[shown in Figs. 9(a–d) for all sands] as the pile penetrated further not only increasing the area of the interface zone but also causing further contraction. The drop in skin friction is even more dramatic in this case because of the model pile being in effect a bored pile. As a result the soil adjacent to the interface can dilate on loading, whereas for a driven pile the interface soil has already flowed around the pile tip and undergone dilation in the process. A similar brittle shaft response was observed by Lehane et al. (2005). It can be seen that the peak skin friction is closely related to the lateral stress such that in Figs. 9(a and c) the peak values are almost identical for a lateral stress of 100 kPa (Table 2) while in Figs. 9(b and d) a lateral stress increase first to 200 kPa and then to 300 kPa caused a considerable increase in the peak skin friction. In this case the increase in end bearing stresses may also have caused a corresponding increase in the lateral stresses at the base of the pile.

Although there was a notable difference between the peak values of skin friction at low displacements, this difference had all but disappeared at $S/D=3$. At higher lateral stresses, however, it can be seen that the less crushable Toyoura sand generated higher skin frictions. It can be argued that as the lateral effective stress around the pile increased so the arching effect in the angular skeletal particles also increased and this combined with the marked interface zone of degraded particles adjacent to the pile at $\sigma_v=\sigma_h=300$ kPa led to the reduced skin friction seen for the carbonate sands in Fig. 9(d). In summary, the more contractile behavior of the carbonate sands leads to a more dramatic loss of normal stress on the pile shaft due to the contracting interface zone. In these tests, which have a stress controlled radial stress boundary, the contraction causes the imposed stress to arch around the pile.

In each test unloading occurred at $S/D=1.0$ and 2.0. In each case the unloading and reloading stiffness was very high and the yield point was very sharp as the pile reached the previous skin friction achieved before unloading. Reloading did not give the same peak in skin friction as was observed under initial loading. It is thought that the sleeve of crushed material formed around the pile as has been previously observed by White and Bolton (2004) was causing this kind of behavior. In the case of a driven pile, therefore, one would not expect a sharp peak in the skin friction since the soil adjacent to the pile had been previously sheared. However one might expect to see this in a bored pile.

Soil Behavior around Pile

In order to observe the behavior of the soil around the pile an additional three samples of Chiibishi sand were produced with layers of colored particles added to the sand as it was being formed. After testing, the samples were moistened to generate sufficient suction for them to be self-supporting and they were then sectioned using a straight edge and photographed. The testing conditions for the sectioned samples were $\sigma_v=\sigma_h=400$ kPa, $K=1.0$, and $D_r=90\%$ and the variations in end bearing and skin friction with settlement for the sample loaded to $S/D=3.0$ are shown in Figs. 10(a and b).

Pile Tip Soil Behavior

The samples of Chiibishi sand were sectioned and photographed at $S/D=0.5$, 1.0, and 3.0 [Figs. 11(a–c)]. In addition samples of Dogs Bay and Toyoura sand were sectioned at $S/D=1.0$ [Figs. 11(d and e)]. The distance between the colored layers was 10 mm.

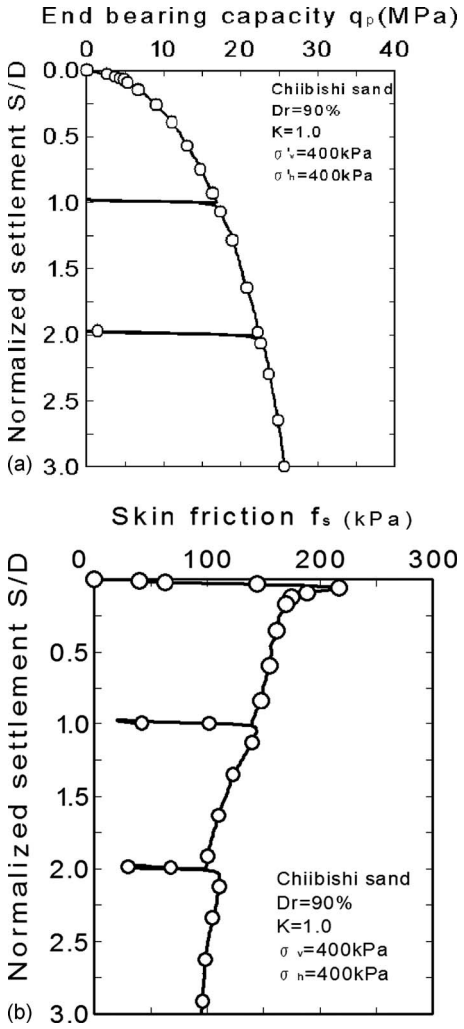

Fig. 10. (a) End bearing capacity versus normalized settlement, $\sigma_v=400$ kPa, $K=1.0$, Chiibishi sand; (b) skin friction versus normalized settlement, $\sigma_v=400$ kPa, $K=1.0$, Chiibishi sand

It can be seen in Figs. 11(a–c) for Chiibishi sand that a spherical plastic zone was formed at the base of the pile which expanded with increasing S/D and a degraded layer of broken particles developed around the pile as S/D increased. Comparison of Figs. 11(b, d, and e) for $S/D=1.0$ shows that slight heave occurred in the layers adjacent to the pile for Toyoura sand but this was suppressed in the case of the two carbonate sands. In the case of Toyoura sand the harder silica grains were displaced sideways generating the heave. In the case of the carbonate sands the crushing caused a densification and corresponding contraction of the sand and thus eliminated the heave. It can be seen in Fig. 11(c) that even at a displacement $S/D=3.0$ there is still no evidence of heave for the Chiibishi sand. There are clearly two distinct mechanisms of failure for crushable and relatively hard grained materials. In the case of the crushable sand there does not appear to be any evidence of the formation of a Meyerhof (1976) type of failure mechanism of shear bands extending away from the pile tip, which is commonly cited in text books and underlies the classical bearing capacity solutions for end bearing. The absence of distinct shear bands indicated that the penetration mechanism is more closely approximated by a continuum cavity expansion type of analysis. However, the deformation pattern also indicates that the pile penetration is partly accommodated by volume con-

J. Geotech. Geoenviron. Eng., 2009, 135(7): 901-913

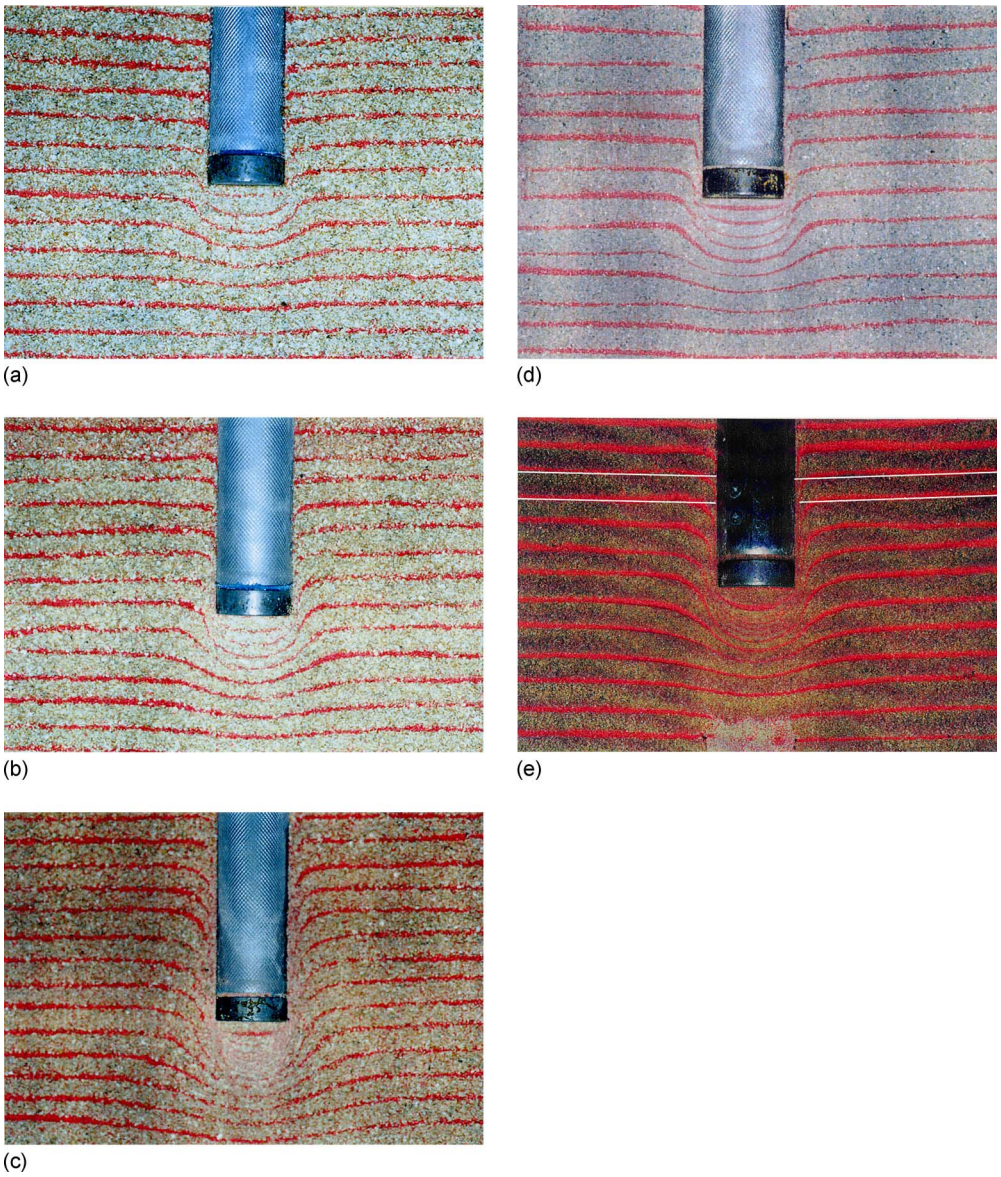

Fig. 11. (a) Chiibishi sand $S/D=0.5$; (b) Chiibishi sand $S/D=1.0$; (c) Chiibishi sand $S/D=3.0$; (d) Dogs Bay sand $S/D=1.0$; and (e) and Toyoura sand $S/D=1.0$

traction in the near field as well as continuum shearing toward the far field. It is therefore important to introduce a crushability factor into the calculation of bearing capacity.

Pile Shaft Soil Behavior

In order to investigate the shearing zone around the pile in carbonate sands an additional sample of Chiibishi sand was stripped just after the peak skin friction was reached with $S/D=0.05$. In this case the sample was consolidated to 400 kPa with a K_0 value of 1.0. Fig. 12 shows the layers after sectioning and Fig. 13 then shows a schematic of the pile layer deformations. Measurements were taken of r_m, the radius of layer drawdown, and δ, the magnitude of layer drawdown at the pile face. Table 3 shows these values averaged for all layers shown in Fig. 12. Similar measurements were taken for the Chiibishi sand at $S/D=1.0$ and 3.0 but above the initial location of the base of the pile. Displacement measurements were averaged on layers above the initial location of the base of the pile in order to eliminate the distortions due to pile end bearing penetration. The resulting displacement of the layers due to skin friction alone was very small with δ/D values of 0.05–0.06 and r_m/r_0 with values of 2.3–2.7. This indicates that a narrow annular slip plane was formed close to the pile and very

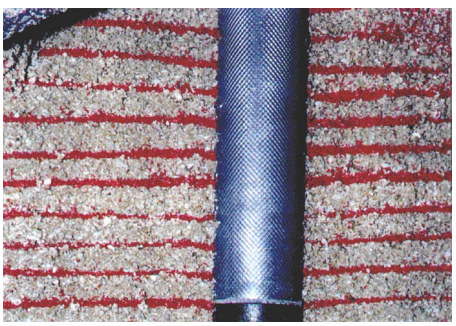

Fig. 12. Chiibishi sand $S/D=0.05$

J. Geotech. Geoenviron. Eng., 2009, 135(7): 901-913

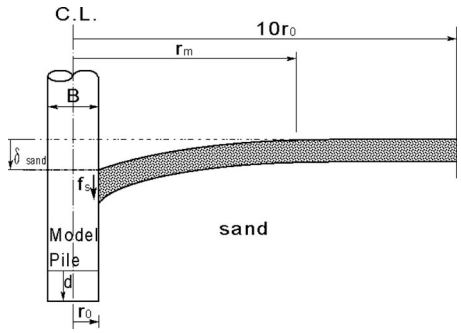

Fig. 13. Schematic of pile layer deformations

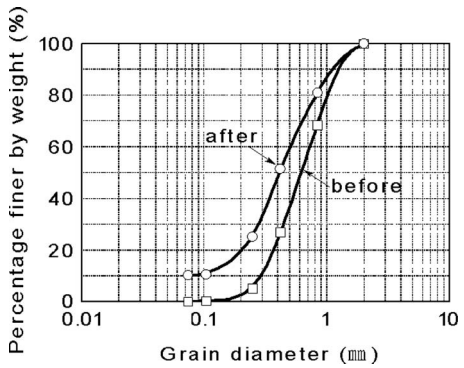

Fig. 15. Particle-size distribution curves for Section D2

little shear strain was transmitted to the surrounding soil. Coop et al. (2004), using a ring shear apparatus on annular soil samples, demonstrated that particle breakage during shear continued over very large shear strains. An increase in fines close to the pile was also observed in these model pile tests. As the grains in the annulus close to the pile continued to break after the peak value of skin friction f_s, the magnitude of the skin friction reduced. Similar tests performed by Tanaka et al. (1995) using a smooth pile caused even smaller strains in the surrounding soil.

Particle Crushing in Surrounding Soil

In order to investigate the soil crushing surrounding the pile, the specimen was dismantled carefully using 4 cm high annular rings with diameters 100, 60, 40, and 20 mm. Fig. 14 is a cross section showing the method of sectioning the sand. Each area shown in Fig. 14 represents an annular ring of soil. Each annulus was sieved and compared with the original particle-size distribution of the sand. The sample was moistened to make it self-supporting during the sectioning process.

The degree of particle crushing can be assessed by comparing particle-size distribution curves before and after testing. There are several methods which include integrating the area between the particle-size distribution curves (Hardin 1985), summing the change in particle sizes, or measuring the difference in specific surface (Tarantino and Hyde 2005). The authors in this case used the method proposed by Marsal (1965) who defined the degree of particle crushing as the peak percentage difference between the particle-size distribution curves. The percentage finer before testing is calculated for each sieve as $f_1, f_2 \ldots .. f_n$, from the largest to smallest sieve diameter, and after testing as $f_1', f_2' \ldots .. f_n'$. Individual differences are calculated as $f_1' - f_1 \ldots .. f_n' - f_n$.

The breakage factor is then defined as

$$B_M = \sum_{i=1}^{k} |f_i' - f_i| = \sum_{i=k+1}^{n} (f_i' - f_i) \quad (1)$$

where n=total number of sieves; and k=sieve number giving the maximum change before and after testing (i.e., sieve No. 3 in Figs. 15 and 16). The magnitude of B_M is related to the degree of crushing. Fig. 15 shows the typical particle-size distribution (PSD) curves before and after testing for Section D2 (Fig. 15) with $K=1$ and $\sigma_v'=400$ kPa. Fig. 16 in effect shows the relative vertical distance between the PSD curves for each particle size. The peak value can be seen clearly in this figure. The B_m values for each section are plotted in Fig. 14 against the normalized vertical distance from the base of the pile Y/D and the radial distance from the edge of the pile X/D for a pile penetration $S/D=1.0$ in Figs. 17(a and b). The B_M value is largest at the pile

Table 3. Sand Layer Displacements

S/D	r_0 (mm)	δ_{sand} (mm)	r_m (mm)	δ/D	r_m/r_0
0.05 (f_{max})	15	1.5	34	0.05	2.3
1.0	15	18	38	0.06	2.5
3.0	15	19	41	0.06	2.7

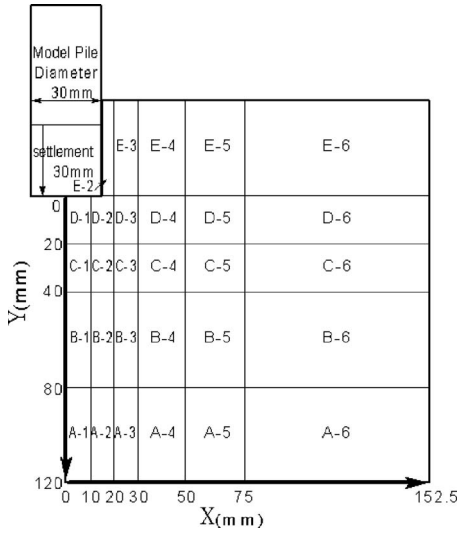

Fig. 14. Sample sectioning scheme

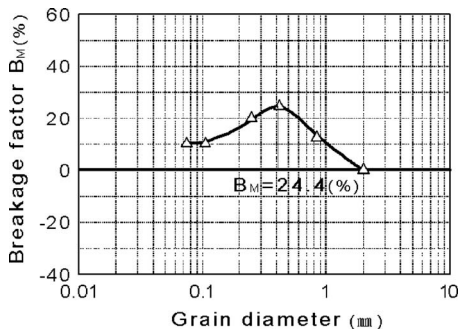

Fig. 16. Marsal breakage factor B_M

J. Geotech. Geoenviron. Eng., 2009, 135(7): 901-913

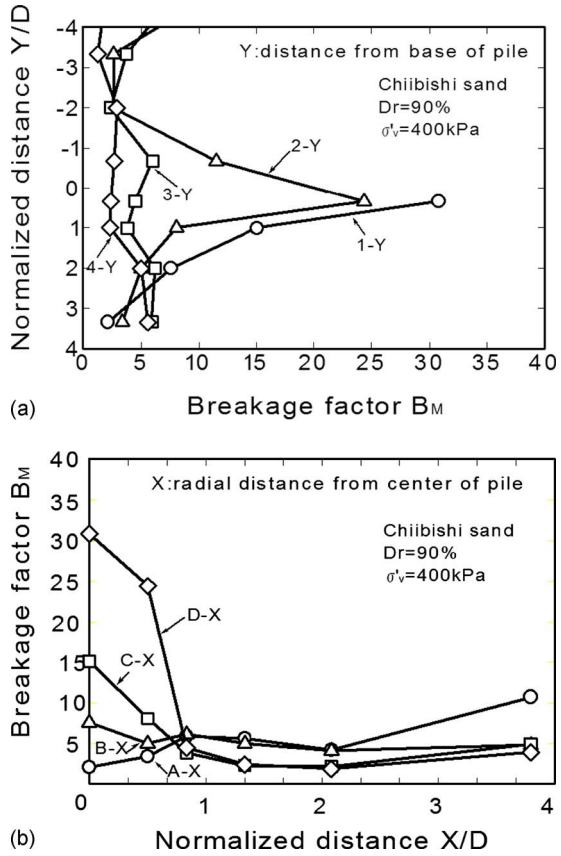

Fig. 17. (a) Breakage factor B_m relative to base of pile; (b) breakage factor B_m relative to radial distance from center of pile

tip where both Y and X are zero. In each case, large values of B_M are limited to a radius of about one pile diameter which corresponds to the crushing zone observed in Fig. 11. Using the relations shown in Fig. 17, contours of the breakage factor B_M are plotted for $S/D=1.0$, $\sigma'_v=400$ kPa, and $K_0=1$ in Fig. 18. Superimposed on this figure are the profiles of the deformed colored layers taken from the equivalent photograph and plotted as broken lines. It can be seen that the B_M values are largest at the center and in the vicinity of the pile, the soil immediately below the pile having suffered the greatest degree of crushing. The contours for B_M between 10 and 30 form approximately concentric hemispheres around the base of the pile. The curves for deformation and crushing are only loosely related in this figure.

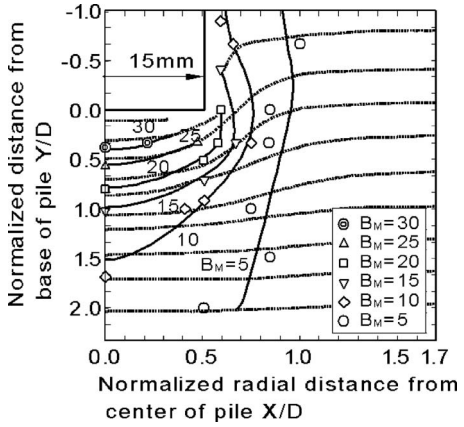

Fig. 18. Breakage factor contours

Bearing Capacity Modification Factors

Previous work by Yasufuku et al. (1994) proposed the following equation for bearing capacity at a displacement of 100% of the pile diameter, taking into account soil compressibility

$$q_{p100\%} = N_q^* \sigma'_v \tag{2}$$

where

$$N_q^* = F_f \,.\, N_q \tag{3}$$

$$N_q = \tan^2\left(\frac{\pi}{4} + \frac{\phi'}{2}\right)\exp(\pi \tan \phi') \tag{4}$$

σ'_v=vertical effective stress; and F_f=factor which is a function of the isotropic compressibility decreasing linearly with $\log C'_p$ where

$$C'_p = \frac{\Delta e}{\Delta(\ln \sigma'_m)} \tag{5}$$

where e=void ratio; and σ'_m=mean normal effective stress.

However Yasufuku's model pile tests were terminated at a maximum S/D of 1.0 which is insufficient settlement to identify the limiting base resistance. The writers have extended this work by obtaining end bearing values $q_{p100\%}$. $q_{p200\%}$ and $q_{p300\%}$ from the model pile tests at $S/D=1.0$, 2.0, and 3.0, respectively, and the corresponding $N_q^*=q_p/\sigma'_v$ values are shown in Figs. 19(a–c), varying with vertical stress for Chiibishi, Dogs Bay, and Toyoura sands. Reissner, (1924) N_q value, calculated using a characteristic ϕ' determined at maximum compressive volumetric strain, is shown in these figures for comparison. The characteristic values of ϕ' used were 42.5° (Chiibishi sand), 36° (Dogs Bay), and 31.5° (Toyoura sand). These are far lower than the peak values shown in Fig. 5 and did not vary with confining pressure. The values of N_q^* obtained from the model tests decreased with effective vertical stress σ'_v and this was more marked for the carbonate sands. A comparison of Reissner's N_q values with those determined at $S/D=1.0$ shows a sixfold increase for Toyoura sand. On the other hand, N_q is actually less than the Reissner (1924) value for Chiibishi and Dogs Bay sands at values of confining pressure in excess of 100 and 250 kPa, respectively. For $S/D=3.0$, these confining pressures are 200 and 300 kPa, respectively. Use of Reissner's equation leads to underestimation in the case of Toyoura sand but a considerable overestimation for carbonate sands at higher stress levels. It can be seen in Fig. 19 that N_q^* actually increases with increasing penetration S/D.

A new modification factor F_f^* has been derived in terms of the mean normal stress σ'_m such that

$$q_p = S_D F_f^* N_q \sigma'_m \tag{6}$$

where

$$F_f^* = F_f\left(\frac{3}{2K_0 + 1}\right) \tag{7}$$

and S_D=factor for penetrations higher than $S/D=1.0$.

Figs. 20(a–c) show the variation of the modification factor F_f^* with mean normal effective stress.

J. Geotech. Geoenviron. Eng., 2009, 135(7): 901-913

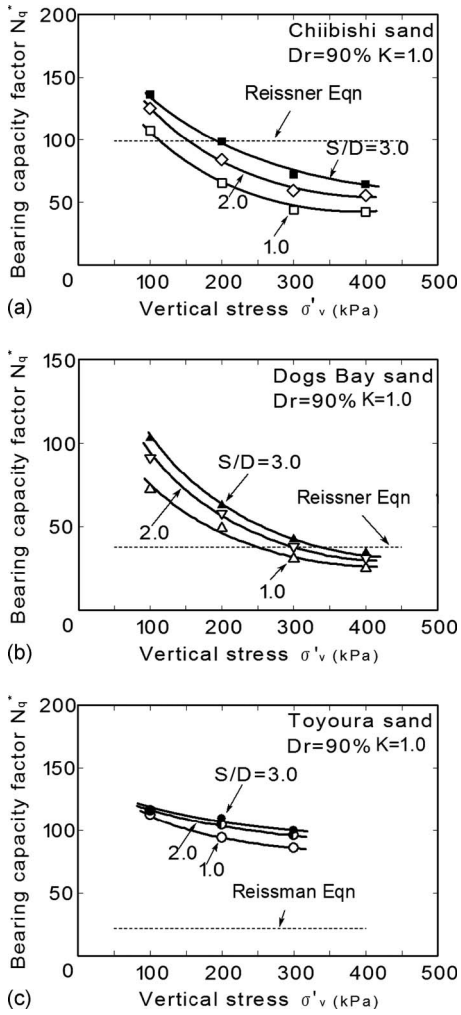

Fig. 19. (a) Bearing capacity factor N_q^* versus σ_v for Chiibishi sand; (b) bearing capacity factor N_q^* versus σ_v for Dogs Bay sand; and (c) bearing capacity factor N_q^* versus σ_v for Toyoura sand

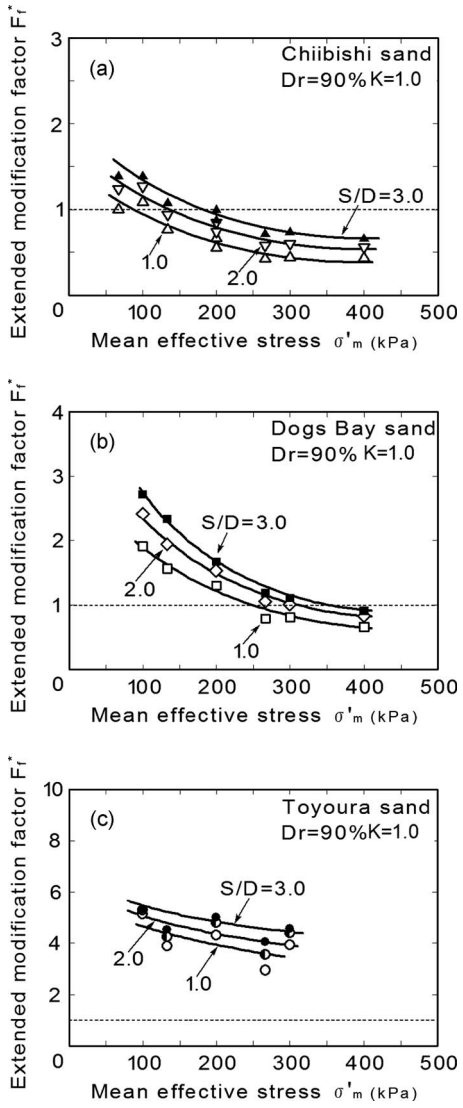

Fig. 20. (a) Extended modified factor F_f^* for Chiibishi sand; (b) extended modified factor F_f^* for Dogs Bay sand; and (c) extended modified factor F_f^* for Toyoura sand

F_f^* is shown in Figs. 21(a–c) to be a function of both compressibility C_p' and penetration S/D with values less than unity for C_p' values in excess of 0.025 for $S/D=1.0$ and 0.04 for $S/D=3.0$. The lines from Figs. 21(a–c) are redrawn in Fig. 21(d). It can be seen that the modification factor F_f^* increases as S/D increases. Driven piles which plug during installation, or closed-ended piles, would mobilize the resistance evident at large S/D values since the load test represents a continuation of the deformation accumulated during the installation phase. In this case an end bearing capacity derived using the curve for $S/D=3.0$ would seem reasonable. On the other hand, the allowable settlement of a bored pile is likely to be much lower than $S/D=1.0$ and thus the use of the curve for $S/D=1.0$ would potentially be optimistic.

Conclusions

Model pile tests have been carried out in two skeletal carbonate sands and a standard silica sand with the aim of examining the variation of skin friction and end bearing capacities with degree of penetration. Consolidated drained triaxial tests were carried out on the three sands. The peak deviator stress was reached at an axial strain of $\leqslant 5\%$ for the silica Toyoura sand, in contrast to the carbonate sands where peak stresses were reached at axial strains of more than 20% in some cases, which together with a decreasing tendency to dilate is an indicator of the greater relative grain crushing. It should be noted that mobilization of the strength of crushable soils requires a much higher strain level while at the same time the end bearing pressure on the model piles exceeded 10 MPa in all cases and one would therefore expect considerable particle breakage particularly in the more crushable materials. Both factors are important considerations in pile bearing capacity problems.

The peak skin friction for all sands occurred at a normalized displacement S/D of less than 0.1. At this point the carbonate sands generally had lower skin friction values than the silica sand. Further displacement caused a rapid decrease in skin friction for all three materials. Although there was a notable difference between the peak values of skin friction at low displacements, this difference had all but disappeared at $S/D=3$. At higher lateral stresses, however, the less crushable Toyoura sand generated higher skin frictions. It can be argued that the interface zone of degraded particles adjacent to the pile contracts especially for

J. Geotech. Geoenviron. Eng., 2009, 135(7): 901-913

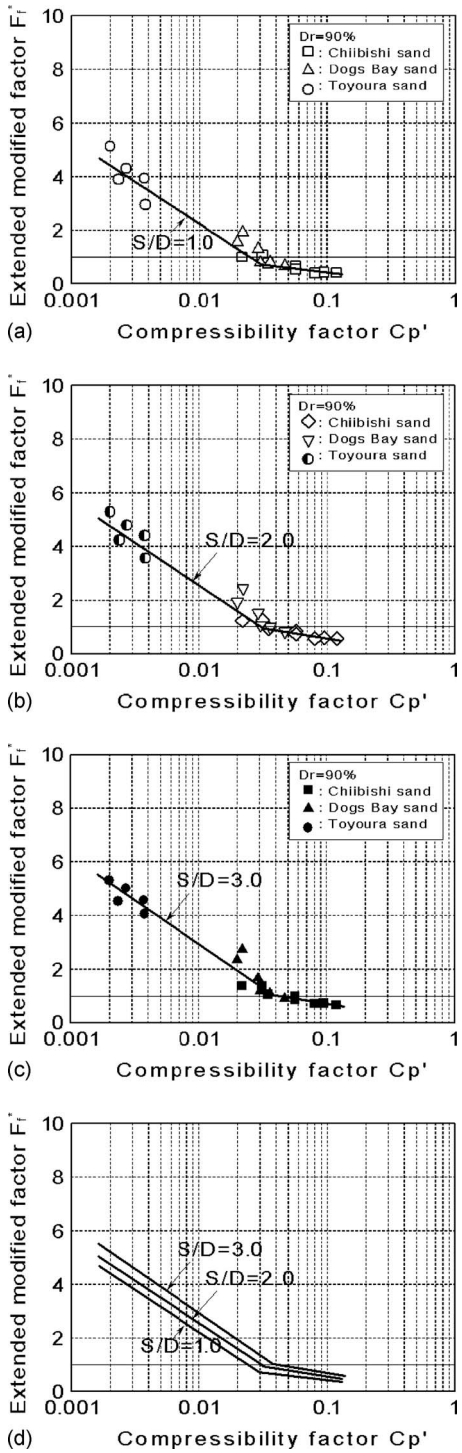

Fig. 21. (a) Extended modified factor F_f^* versus compressibility C_p', $S/D=1.0$; (b) extended modified factor F_f^* versus compressibility C_p', $S/D=2.0$; (c) extended modified factor F_f^* versus compressibility C_p', $S/D=3.0$; and (d) extended modified factor F_f^* versus compressibility C_p'

carbonate sands causing the radial stresses on the pile to drop and leading to the reduced skin friction seen for the carbonate sands. At the same time equilibrium with the boundary stresses is maintained by a rise in circumferential stresses which arch around the pile.

The unloading and reloading stiffness was very high but reloading did not give the same peak in skin friction as was observed under initial loading. In the case of a driven pile therefore one would not expect a sharp peak in the skin friction but one might expect to see this in a bored pile.

Samples of Chiibishi sand were sectioned and photographed. It was observed that a spherical plastic zone was formed at the base of the pile which expanded with increasing S/D and a degraded layer of broken particles developed around the pile as S/D increased. Large values of the Marsal particle breakage factor were restricted to a zone extending outwards to one pile radius.

An end bearing capacity modification factor has been proposed which is a function of soil compressibility and degree of penetration. The factor was shown to decrease with increasing soil compressibility and increase with normalized penetration S/D.

References

Airey, D. W., and Fahey, M. (1991). "Cyclic response of calcareous soil from the North-West Shelf of Australia." *Geotechnique*, 41(1), 101–122.

Bolton, M. D. (1986). "The strength and dilatancy of sands." *Geotechnique*, 36(1), 65–78.

Bopp, P. A., and Lade, P. V. (1997). "Effect of initial density on soil instability at high pressure." *Proc. ASCE*, 123(GT7), 671–677.

Coop, M. R. (1990). "The mechanics of uncemented carbonate sands." *Geotechnique*, 40(4), 607–626.

Coop, M. R., Sorenesen, K. K., Bodas Freitas, T., and Georgoutos, G. (2004). "Particle breakage during shearing of a carbonate sand." *Geotechnique*, 54(3), 157–163.

Garnier, J., Gaudin, C., Springman, S. M., Culligan P. J., Goodings, D., Konig, D., Kutter, B., Phillips, R., Randolph, M. F., and Thorel, L. (2007). "Catalogue of scaling laws and similitude questions in geotechnical centrifuge modelling." *Int. J. Phys. Modell. Geotech.*, 7(3), 1–24.

Golightly, C. R. (1989). "Engineering properties of carbonate sands." Ph.D. thesis, University of Bradford, Bradford, U.K.

Golightly, C. R., and Hyde, A. F. L. (1988). "Some fundamental properties of carbonate sands." *Proc., Int. Conf. on Calcareous Sediments*, Vol. 1, Perth, Australia, 173–184.

Hardin, B. O. (1985). "Crushing of soil particles." *J. Geotech. Engrg.*, 111(10), 1177–1192.

Hyde, A. F. L. (1994). "The modelling of crushable soils." *Proc., Int. Symp. on Pre-Failure Deformation Characteristics of Geo-materials*, Vol. 2, Japanese Society of Soil Mechanics and Foundation Engineering, IS Hokkaido, Japan, 1201–1202.

Hyodo, M., Aramaki, N., Itoh, M., and Hyde, A. F. L. (1996). "Cyclic strength and deformation of crushable carbonate sand." *Soil Dyn. Earthquake Eng.*, 15(5), 331–336.

Hyodo, M., Hyde, A. F. L., and Aramaki, N. (1998). "Liquefaction of crushable soils." *Geotechnique*, 48(4), 527–543.

Hyodo, M., Hyde, A. F. L., Aramaki, N., and Nakata, N. (2002). "Undrained monotonic and cyclic shear behaviour of sand under low and high confining stresses." *Soils Found.*, 42(3), 63–76.

Lehane, B. M., Gaudin, C., and Schneider, J. A. (2005). "Scale effects on tension capacity for rough piles buried in dense sand." *Geotechnique*, 55(10), 709–719.

Marsal, R. J. (1965). "Soil properties—Shear strength and consolidation." *Proc., 6th Int. Conf. on Soil Mechanics and Foundation Engineering*, Montreal, Vol. 3, The University Press, Toronto, 310–316.

McDowell, G. R., and Bolton, M. D. (1998). "On micromechanics of crushable aggregates." *Geotechnique*, 48(5), 667–679.

McDowell, G. R., and Daniell, C. M. (2001). "Fractal compression of soil." *Geotechnique*, 51(2), 173–176.

McDowell, G. R., and Harireche, O. (2002). "Discrete element modelling of yielding and normal compression of sand." *Geotechnique*, 52(4),

299–304.
Meyerhof, G. G. (1976). "Bearing capacity and settlement of pile foundations." *Proc. ASCE*, 102(GT3), 197–228.
Miura, N., and O-hara, S. (1979). "Particle crushing of a decomposed granite soil under shear stress." *Soils Found.*, 19(3), 1–14.
Nakata, Y., Hyde, A. F. L., Hyodo, M., and Murata, H. (1999). "A probabilistic approach to sand crushing in the triaxial test." *Geotechnique*, 49(5), 567–583.
Nakata, Y., Hyodo, M., Hyde, A. F. L., Kato, Y., and Murata, H. (2001a). "Microscopic particle crushing of sand subjected to high pressure one dimensional compression." *Soils Found.*, 41(1), 69–82.
Nakata, Y., Kato, Y., Hyodo, M., Hyde, A. F. L., and Murata, H. (2001b). "One dimensional compression behaviour of uniformly graded sand related to single particle crushing strength." *Soils Found.*, 41(2), 39–51.
Reissner, H. (1924). "Zum erddruckproblem." *Proc., 1st Int. Congress for Applied Mechanics*, Delft, The Netherlands, C. B. Biezeno and J. M. Burgers, eds., Technische Boekandel en Drukkerij J. Waltman Jr., Delft, 295–311.
Tanaka, K., Yasufuku, N., Murata, H., and Hyodo, M. (1995). "Engineering properties of carbonate sands and skin friction of pile in sands." *Proc., Japan Society of Civil Engineers*, Japan Society of Civil Engineers, Tokyo, No. 523/III-32, 99–109 (in Japanese).
Tarantino, A., and Hyde, A. F. L. (2005). "An experimental investigation of work dissipation in crushable materials." *Geotechnique*, 55(8), 575–584.
White, D. J., and Bolton, M. D. (2004). "Displacement and strain paths during plain-strain model pile installation in sand." *Geotechnique*, 54(6), 375–397.
Yasufuku, N., and Hyde, A. F. L. (1995). "Pile end-bearing capacity in crushable sands." *Geotechnique*, 45(4), 663–676.
Yasufuku, N., Tanaka, K., Murata, H., and Hyodo, M. (1994). "End bearing capacity of pile in highly compressible sands and its evaluation." *Proc., Japan Society of Civil Engineers*, Japan Society of Civil Engineer, Tokyo, No. 505/III-29, 191–200 (in Japanese).